



HAL
open science

A satellite and model-based assessment of the 2003 Russian fires : Impact on the Arctic region

Sylvia Generoso, Isabelle Bey, Jean-Luc Attié, Francois-Marie Breon

► To cite this version:

Sylvia Generoso, Isabelle Bey, Jean-Luc Attié, Francois-Marie Breon. A satellite and model-based assessment of the 2003 Russian fires : Impact on the Arctic region. *Journal of Geophysical Research: Atmospheres*, 2007, 112, pp.D15302. 10.1029/2006JD008344 . hal-00561395

HAL Id: hal-00561395

<https://hal.science/hal-00561395>

Submitted on 28 Oct 2020

HAL is a multi-disciplinary open access archive for the deposit and dissemination of scientific research documents, whether they are published or not. The documents may come from teaching and research institutions in France or abroad, or from public or private research centers.

L'archive ouverte pluridisciplinaire **HAL**, est destinée au dépôt et à la diffusion de documents scientifiques de niveau recherche, publiés ou non, émanant des établissements d'enseignement et de recherche français ou étrangers, des laboratoires publics ou privés.

A satellite- and model-based assessment of the 2003 Russian fires: Impact on the Arctic region

Sylvia Generoso,¹ Isabelle Bey,¹ Jean-Luc Attié,² and François-Marie Bréon³

Received 13 December 2006; revised 17 April 2007; accepted 2 May 2007; published 2 August 2007.

[1] In this paper, we address the issues of the representation of boreal fires in a global chemistry and transport model (GEOS-Chem) as well as their contribution to the Arctic aerosol optical thickness and black carbon (BC) deposition, with a focus on the 2003 Russian fires. We use satellite observations from the MOPITT, POLDER and MODIS sensors to evaluate the model performances in simulating the fire pollution export over the North Pacific. Our results show that aerosol and carbon monoxide (CO) outflow is best reproduced in our model when fire emissions are (1) increased to 72 Tg for CO, 0.5 Tg C for BC, and 5.3 Tg C for organic carbon over the entire fire season; (2) prescribed on a daily basis; and (3) injected up to 4.5 km in July and August. The use of daily, rather than monthly, biomass burning emission inventories improves significantly the representation of the aerosol outflow, but has little impact on CO. The injection of fire emissions above the boundary layer influences both the CO and aerosol columns but only during the late fire season. The model improvements with respect to the standard configuration induce an increase of a factor up to 2 on the aerosol optical thickness and the mass of BC deposited in the Northern Hemisphere. According to our improved simulation, the 2003 Russian fires contributed to 16–33% of the aerosol optical thickness and to 40–56% of the mass of BC deposited, north of 75°N in spring and summer. They contribute to the aerosol optical thickness by more than 30% during the days of Arctic haze events in spring and summer.

Citation: Generoso, S., I. Bey, J.-L. Attié, and F.-M. Bréon (2007), A satellite- and model-based assessment of the 2003 Russian fires: Impact on the Arctic region, *J. Geophys. Res.*, 112, D15302, doi:10.1029/2006JD008344.

1. Introduction

[2] Remote sensing observations show that forest fires in boreal regions can have a large impact on the Northern Hemisphere atmospheric trace gas and aerosol loadings [e.g., Edwards *et al.*, 2004]. Even though the surfaces of burned area in boreal regions are smaller than those in tropical regions, the amount of biomass consumed is significant because boreal forest and peatland soils contain a deep layer of organic matter [Kasischke and Bruhwiler, 2002; Kasischke *et al.*, 2005]. These fires induce a large variability in the atmospheric pollutant emissions and partly drive the temporal variability of the Northern Hemisphere trace gas and aerosol burdens [e.g., Wotawa *et al.*, 2001; Langenfelds *et al.*, 2002; van der Werf *et al.*, 2004]. The boreal fire emissions tend to increase over the recent decades [Lavoué *et al.*, 2000] and this is expected to continue in the future as a result of the predicted warmer

and dryer conditions [Flannigan *et al.*, 2000, 2005]. Recent studies have suggested that the observed changes in climate have already influenced the boreal fire activity (i.e., increase in intensity, frequency and duration of the fire season) [Gillett *et al.*, 2004; Westerling *et al.*, 2006]. This is likely to have important implications in terms of terrestrial carbon dioxide, trace gas and aerosol emissions and may correspond to an important feedback process between climate and the biosphere [e.g., Randerson *et al.*, 2006].

[3] Recent studies have also emphasized the significant influence of the boreal forest fires on the Arctic aerosol burden in summer [e.g., Koch and Hansen, 2005; Iziumon *et al.*, 2006; Stohl, 2006; Stohl *et al.*, 2006]. The Arctic region, which is particularly sensitive to climate change [e.g., Arctic Climate Impact Assessment, 2004; Kaplan and New, 2006], experiences enhanced aerosol loads that are largely attributed to the long-range transport of pollution from urban, industrial and biomass burning sources in the mid-northern latitudes [e.g., Shaw, 1995]. Once in the Arctic atmosphere, aerosols can modify the regional circulation patterns and the hydrological cycle [Rinke *et al.*, 2004] and increase the snow absorption, resulting in a strong impact on the surface albedo and evaporation rate [e.g., Clarke and Noone, 1985; Hansen and Nazarenko, 2003].

[4] The impact of forest fires on atmospheric pollutant loadings (and thus on climate) remains uncertain. Global

¹Laboratoire de Modélisation de la Chimie Atmosphérique, Ecole Polytechnique Fédérale de Lausanne, Lausanne, Switzerland.

²Laboratoire d'Aérodynamique, Toulouse, France.

³Laboratoire des Sciences du Climat et de l'Environnement, Institut Pierre Simon Laplace, Gif-sur-Yvette, France.

models of chemistry and transport are particularly well suited to provide useful information. However, there are still some large uncertainties in the representation of biomass burning in current models, in particular in terms of emission amount and variability. Although the monitoring of fires from space can be used to better represent their spatial and temporal variations in models [e.g., *Schultz, 2002; Duncan et al., 2003; Generoso et al., 2003; van der Werf et al., 2003; Hoelzemann et al., 2004*], there are still large uncertainties in the satellite-derived emission estimates [e.g., *Kasischke et al., 2003; Kasischke and Penner, 2004; Ito and Penner, 2005*]. In addition, the injection height of the products from fires is generally not specified, e.g., most global models of chemistry and transport distribute emissions within the planetary boundary layer (PBL), while *Lavoué et al. [2000]* argue that particles can be injected well above. Recent observations of intense Canadian forest fires indicated that smoke can even penetrate the stratosphere [*Fromm and Servranckx, 2003; Fromm et al., 2005*].

[5] Several spaceborne instruments monitored a large amount of aerosols and CO emitted during the 2003 Russian fires [*Edwards et al., 2004*]. Aircraft measurements also revealed enhanced CO concentrations in the upper troposphere over northeast Asia from April to August 2003, with maxima over 500 ppbv and a peak up to 850 ppbv in early June 2003 [*Nedelec et al., 2005*]. *Damoah et al. [2004]* reported circulation around the Northern Hemisphere of plumes from the Russian fires in May 2003. *Jaffé et al. [2004]* and *Bertschi and Jaffé [2005]* indicated that such pollution episodes had a significant influence on the regional air quality of northwest America. Enhanced free tropospheric aerosols were also observed by lidars in Europe during that time [*Mattis et al., 2003; Müller et al., 2005*]. There are also some evidences that those fire events influenced the Arctic atmosphere [*Generoso et al., 2007*].

[6] In this study, we use a global chemical transport model to quantify in a comprehensive way to what extent various processes (including strength, temporal resolution and injection heights of the fire emission, deposition) affect the long-range transport of aerosols and carbon monoxide (CO) emitted during boreal fires. Sensitivity simulations of the coupled aerosol-oxidant system were performed and analyzed in light of several satellite data sets including aerosol products from both the Polarization and Directionality of the Earth Reflectance (POLDER) and the Moderate-resolution Imaging Spectroradiometer (MODIS), and CO products from the Measurement of Pollution In The Troposphere (MOPITT). We examined both CO and aerosol distributions as they are key atmospheric components that influence both climate and air quality and can provide complementary information as regard to the understanding of fire emissions and transport [*Edwards et al., 2004*]. We then use our findings to provide an improved representation of the 2003 Russian fires and of their export to the North Pacific, and to quantify their contribution to the Arctic aerosol loads. Note that biomass burning leads to the release of particles that are mostly in the fine mode (radius smaller than 1 μm) [e.g., *Kaufman et al., 2002*]. Their contribution to the total aerosol optical thickness may be hidden in the presence of coarse particles (e.g., as during dust events), and

therefore we restricted our analysis of the aerosol distribution to the fine mode fraction.

[7] Section 2 presents the satellite observations used in this study and the GEOS-Chem model; simulated and observed CO and aerosol distributions are compared in the frame of the east Asian and North Pacific regions during spring and summer 2003 in section 3. Section 4 describes the model sensitivity analysis and presents the results in terms of the different processes influencing fire emission and plume export to the Pacific. Section 5 shows the contributions of the 2003 Russian fires to the Arctic aerosol optical thickness and BC deposition. Section 6 presents a summary and our conclusions.

2. Data and Method

2.1. Aerosol Satellite Products: POLDER and MODIS

[8] The Polarization and Directionality of the Earth Reflectance (POLDER) instrument is a spaceborne radiometer developed by the French space agency (Centre National d'Études Spatiales) [*Deschamps et al., 1994*], launched aboard the Advanced Earth Observation Satellite (ADEOS 1 and 2) in 1996 and 2003. The POLDER orbits have a local overpass time around 10:30 am and provide a quasi-global coverage every day, although clouds often prevent aerosol retrieval [*Deschamps et al., 1994*]. POLDER measures the polarization and directionality of the solar radiation reflected by the Earth, which allows the monitoring of aerosol characteristics, derived separately over land and ocean using independent algorithms. Both the total aerosol optical thickness (AOT) and the fine mode aerosol optical thickness (referred to as AOT_f) are retrieved over the oceans [*Deuzé et al., 2000*]. POLDER can retrieve optical characteristics of particles whose radius is smaller than 0.5 μm (fine mode) over land [*Deuzé et al., 2001*] using its polarization capabilities, while larger particles generate low polarization and cannot be observed with this technique. The data set used in this study is from the POLDER-2 mission, which covered the period from April to October 2003, and consists of daily AOT_f at 865 nm ($\text{AOT}_{f,865}$) regridded in this study at the $2^\circ \times 2.5^\circ$ model resolution. Initial validation of the POLDER products were presented by *Goloub et al. [1999]*, *Deuzé et al. [2000]* and *Deuzé et al. [2001]*. Several improvements were applied to the algorithms, as described for instance by *Herman et al. [2005]*.

[9] The Moderate-resolution Imaging Spectroradiometer (MODIS) on board the Terra satellite and developed by the National Aeronautics Space Administration (NASA) has the same local overpass time than POLDER. MODIS provides multispectral measurements that are used to retrieve aerosol properties over land and ocean using separate algorithms. Retrievals over ocean include AOT (at seven wavelengths from 0.43 to 2.13 μm) and AOT_f (radius smaller than 0.5 μm) [*Tanré et al., 1997; Remer et al., 2002*]. Over land, aerosol retrieval is possible over dark surfaces but not available over bright land (i.e., desert or snow/ice-covered surfaces) [*Kaufman et al., 1997; Chu et al., 2002*]. The MODIS data used in this study come from Terra Collection 005 and consist in daily AOT_f at 550 nm ($\text{AOT}_{f,550}$) globally gridded at $1^\circ \times 1^\circ$ horizontal resolution, and regridded here at the $2^\circ \times 2.5^\circ$ model resolution. Comparisons to Aerosol

Robotic Network (AERONET) ground-based measurements show that, the MODIS AOT (τ) are accurate to within $\pm 0.05 \pm 0.15 \tau$ over land and $\pm 0.03 \pm 0.05 \tau$ over ocean [Remer et al., 2005].

[10] As remote sensing aerosol products can present high bias especially over land, we used two of the currently available products. A general good agreement is found between the POLDER and MODIS products used in this study [Gérard et al., 2005]. Discrepancies are found mostly in the presence of large nonspherical particles (e.g., dust), but this is not expected to be the case here since biomass burning aerosols are mostly in the fine mode. Note that a recent study by Smirnov et al. [2006] indicates that satellite retrieved aerosol optical thickness (in this case MODIS products) are generally higher than ground-based measurements.

2.2. CO Satellite Products: MOPITT

[11] The Measurement Of air Pollution In The Troposphere (MOPITT) instrument is a thermal and near-infrared nadir-viewing gas correlation radiometer launched aboard the NASA Terra platform (December 1999). The instrument allows the retrieval of CO vertical profiles and provides a near-global coverage of the Earth within three days. MOPITT retrievals are derived from the maximum likelihood method [Rodgers, 2000] and is therefore a statistical combination of the measurements and a priori CO information [Deeter et al., 2003]. In this study we used the Level 2 Version 3 products, which consist in retrieved CO mixing ratio profiles and total column for all cloud-free scenes. The CO mixing ratio are reported at the seven pressure levels: surface, 850, 700, 500, 350, 250, 150 hPa. However, for a given vertical profile no more than 2 levels provide independent pieces of information, in general [Heald et al., 2003b; Deeter et al., 2004]. Emmons et al. [2004] report error of $0.9 \pm 10.4\%$ at 500 hPa, $1.6 \pm 10.1\%$ at 350 hPa and $-0.5 \pm 12.1\%$ for the data acquired after August 2001, although local biases could be somewhat larger. Further information about MOPITT retrieval method, vertical resolution and validation are given by Deeter et al. [2003], Deeter et al. [2004] and Emmons et al. [2004]. We restrict our analysis to the MOPITT data obtained with an a priori contribution of less than 40% at 500 hPa.

2.3. GEOS-Chem

[12] We used the GEOS-Chem chemical and transport model (CTM) (<http://www-as.harvard.edu/chemistry/trop/geos/>), version v7-02-03, to conduct global three-dimensional simulations of coupled oxidant-aerosol chemistry for 2003 with a $2^\circ \times 2.5^\circ$ horizontal resolution and 30 vertical levels. The model is driven by assimilated meteorology from the Goddard Earth Observing System (GEOS-4) of the NASA Global Modeling and Assimilation Office (GMAO), which includes winds, temperature, surface pressure, water content, clouds, precipitation, convective mass fluxes, mixed layer depth and surface properties with a 6-hour temporal resolution (3-hour for surface variables and mixing depths). The model simulates the tropospheric ozone-nitrogen oxides (NO_x)-hydrocarbon chemistry [Bey et al., 2001a] as well as the tropospheric aerosol types including sea salts [Alexander et al., 2005], mineral dust [Zender et al., 2003], sulfate-

nitrate-ammonium aerosols [Park et al., 2004], carbonaceous aerosols (including black and primary organic carbon further referred to as BC and OC, respectively) [Park et al., 2003], and Secondary Organic Aerosol (SOA) [Chung and Seinfeld, 2002]. Aerosol and oxidant chemistry simulations interact through sulfate, nitrate and SOA formation, heterogeneous reactions, and aerosol effects on photolysis rate [Martin et al., 2003].

[13] Anthropogenic emissions of NO_x, CO, hydrocarbons and sulphur are based on the Global Emissions Inventory (GEIA) for 1985 [Benkovitz et al., 1996] with updated national inventories scaled to 1998 [Bey et al., 2001a; Park et al., 2004]. Biofuel emissions are estimated from the Yevich and Logan [2003] inventory. Anthropogenic sources of ammonia and carbonaceous aerosols are as described in Park et al. [2004] and Bond et al. [2004], respectively, (except for North American carbonaceous sources, that are from Park et al. [2003]).

[14] Biomass burning emissions for carbonaceous aerosols are derived from the Bond et al. [2004] annual inventory. Climatological inventories of biomass burning trace gas emissions are described by Lobert et al. [1999] and Duncan et al. [2003] for CO, NO_x, alkanes, acetone, and from Park et al. [2003] and Park et al. [2006] for sulphur dioxide and ammonia. These climatological inventories are redistributed in space and time according to the occurrence of open fires detected by the spaceborne Advanced Along Track Scanning radiometer (AATSr) [Arino and Melinotte, 1995] to account for seasonal and interannual variability. The method (including the specific biomass burning regions used) is described in detail by Generoso et al. [2003], except that the fire count data set used in the present study was extended to account for the latest available satellite data (up to 2005). For 2003, our global estimates are 3.34 and 26.3 Tg C for BC and OC, respectively, and 418 Tg for CO.

[15] All aerosols experience dry deposition following the size-dependent scheme of Zhang et al. [2001] for dust and sea salts and a resistance-in-time scheme for the other species as described by Balkanski et al. [1993]. Hydrophilic aerosols are in addition subject to wet deposition, which includes both scavenging in convective updrafts and rain-out/washout from large-scale precipitation [Liu et al., 2001]. A fraction of eighty percent of SOA are assumed to experience wet deposition [Chung and Seinfeld, 2002]. A fraction of twenty and fifty percent of BC and OC, respectively, are emitted as soluble, the hydrophobic part being converted into hydrophilic fraction during particles ageing with an e-folding time of 1.15 days [Cooke et al., 1999; Chin et al., 2002].

[16] The aerosol optical thickness is calculated assuming externally mixed aerosol and lognormal size distributions and as a function of the local relative humidity. The aerosol optical properties and hygroscopic growth factors used in the model are described by Martin et al. [2003]. AOT₈₆₅ and AOT₅₅₀ are calculated online in the model using optical properties at 550 and 865 nm taken from the Global Aerosol Data Set (GADS) [Köpke et al., 1997; Patterson et al., 1977]. To compare model results with the observed fine aerosol optical thickness, we compute a simulated fine aerosol optical thickness which includes all carbonaceous

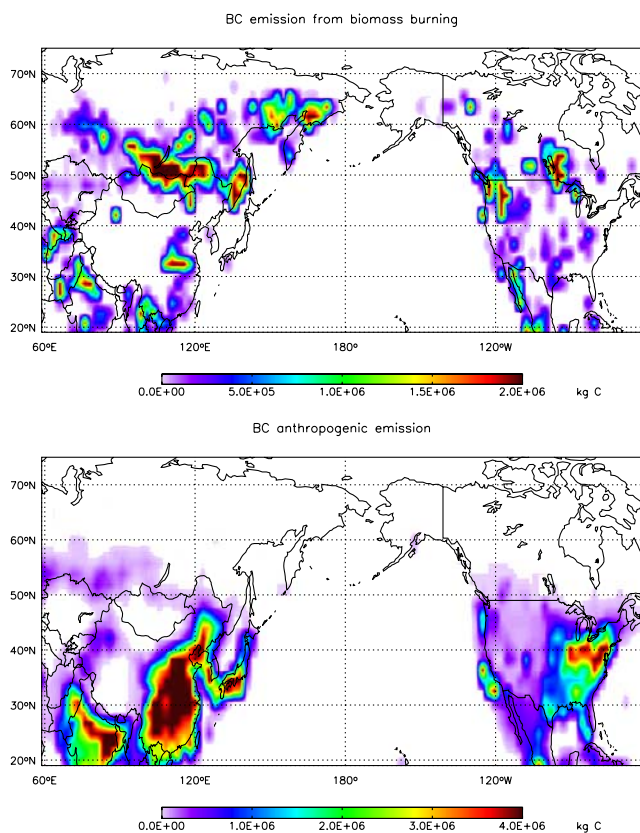


Figure 1. BC emissions between May and August 2003 (top) from biomass burning and (bottom) from biofuel and anthropogenic activities.

aerosols (primary and secondary particles), sulfates and fine sea salts. The effective radius at seventy percent of relative humidity are 0.24, 0.04, 0.10, 1.3 μm for sulfate, black carbon, organic carbon, and fine sea salt, respectively [Martin *et al.*, 2003]. The dust fine fraction is not accounted for in our simulated fine aerosol optical thickness, however we discuss its possible contribution in section 3. The simulated CO columns are compared to MOPITT after transformation by the MOPITT averaging kernel to describe the vertical sensitivity of the instrument to the true CO profiles. MOPITT averaging kernels typically show highest sensitivity in the middle and upper troposphere and low sensitivity in the boundary layer [Deeter *et al.*, 2003].

[17] We conducted a standard simulation as described above starting in July 2002 and analyzed the outputs from May to August 2003. Anthropogenic and biomass burning emissions south of 45°N are mostly from biofuel burning and anthropogenic activities, while wildfire emissions dominate north of 45°N (Figure 1). The sensitivity simulations described in section 4 are performed for the period from April to August 2003, with initial conditions taken from the standard simulation.

3. Aerosol and CO Distributions During May–August 2003 in the North Pacific Ocean

[18] In this section, we compare simulated and observed aerosol optical thickness and CO columns over the Eurasia

area and in the outflow over the North Pacific ocean in the period May–August 2003 and discuss possible reasons for the discrepancies. Enhanced CO and aerosol optical thickness are observed over populated areas (e.g., China and east Asia) and over northeast Asia in association with fires in southeastern Russia (Figure 2). Aerosol loads are more localized over the source regions than CO because of their shorter lifetimes (a few days for aerosols against a few weeks for CO).

[19] Several previous studies have indicated that the GEOS-Chem model reproduces well the CO distributions in the Asian and Pacific areas in 2001 [e.g., Heald *et al.*, 2003b; Heald *et al.*, 2004]. We find that the GEOS-Chem CO columns are well correlated to MOPITT ($r = 0.78$) in the period May to August 2003 but are negatively biased by $-9 \pm 9\%$ (Figure 2), which can be considered as being significant. Note however that Jacob *et al.* [2003] found MOPITT to be positively biased by $6 \pm 2\%$ compared to aircraft in situ measurements in the same region. The model underestimate is larger in the first part of the year (i.e., January–June) (not shown), which may reflect an underestimate of the “background” CO concentrations in the model. We refer to background CO concentrations as to those that result from emissions that occur several weeks before the observations and are well mixed within the atmosphere because of the lifetime of CO. Our biofuel and fossil fuel emissions in China are consistent with estimates derived from aircraft measurements in the Pacific in 2001 by Palmer *et al.* [2003] (154 Tg CO yr⁻¹ versus 168 ± 5 Tg CO yr⁻¹, respectively) and from MOPITT observations [Heald *et al.*, 2004] (154 Tg CO yr⁻¹ including the biomass burning source). On the other hand, severe fire activity has been reported for 2002 in the high northern latitudes. This induced large anomalies in CO in spring over the northern high latitudes (Yurganov *et al.* [2005], and also Figure S1 of the auxiliary material¹), and may explain, to some extent, the model CO underestimate in June 2003 and earlier months.

[20] The simulated aerosol distributions capture the main observed features, in particular in the source region of east Asia (Figure 2). The model reproduces the POLDER and MODIS observations with correlations of $r = 0.65$ and $r = 0.72$, respectively, but POLDER AOT_{f,865} are underestimated by $10 \pm 66\%$ while MODIS AOT_{f,550} are underestimated by $29 \pm 61\%$. The standard model does not reproduce well the amplitude and variability of aerosol loads in the outflow region, especially in July and August (see discussion in section 4). Although Remer *et al.* [2005] reported large uncertainties for the MODIS retrievals over land (see section 2.1), the bias found here are larger than the reported uncertainties of the satellite products. As for CO, our anthropogenic emissions for aerosols are consistent with values reported in the literature. Streets *et al.* [2003], for example, reported annual Chinese fossil fuel and biofuel emissions for carbonaceous aerosols of 0.8 and 2.6 Tg C yr⁻¹ for BC and OC, respectively, while our emissions amount to 1.3 Tg C yr⁻¹ for BC and 2.2 Tg C yr⁻¹ for OC. The aerosol optical thickness underestimate could be due to some extent to a source of SOA in ageing air masses that is

¹Auxiliary materials are available in the HTML. doi:10.1029/2006JD008344.

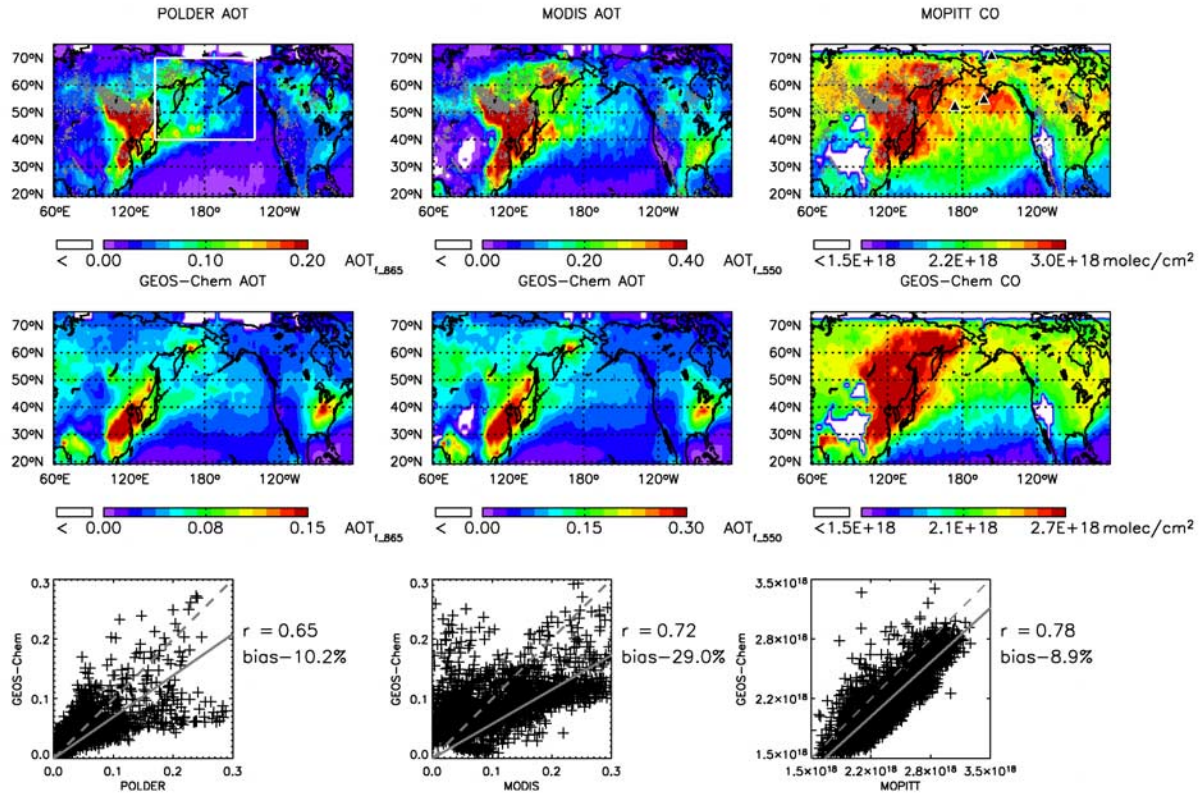


Figure 2. (top) Seasonal mean (May to August 2003) of POLDER AOT_{f_865}, MODIS AOT_{f_550} and MOPITT CO total columns; (middle) corresponding GEOS-Chem aerosol and CO distributions. Note that the color scales are saturated at lower values for the model results (maxima of the color scales decreased by 25% compared to POLDER and MODIS and by 10% compared to MOPITT). (bottom) Scatterplots of seasonal mean POLDER/MODIS/MOPITT versus GEOS-Chem. The white box on the top left plot delimits the region within 40–70°N and 140–220°E used in this study. The black triangles locate the position of the CMDL measurement sites used in this study.

not represented in the model as suggested by *Heald et al.* [2005]. These authors found that the GEOS-Chem model underestimates OC concentrations by a factor 10–100 in the free troposphere (2–7 km) in comparison with concentrations observed during the ACE-Asia campaign. These missing OC concentrations correspond to aerosol optical thickness of up to 0.06 if one considers standard optical properties at 550 nm. In the present study, the average bias between simulated and MODIS AOT_{f_550} over the entire period is of 0.09, and discrepancies reach up to 0.4 (see section 4). Missing SOA formation in the outflow is thus not sufficient to explain our model underestimate. Another possible source of discrepancies can come from the fine fraction of dust which we do not account for in the simulated fine aerosol optical thickness. Figure 3 presents the total daily AOT₅₅₀ observed from MODIS and simulated with the GEOS-Chem model as well as the simulated AOT₅₅₀ of the total dust component (fine and coarse) over the period from May to August 2003. The comparison between the model and the satellite products will be discussed in detail in section 4; here we only focus on the contribution of dust. The simulated AOT₅₅₀ of the total dust component is significant in May, in particular during the

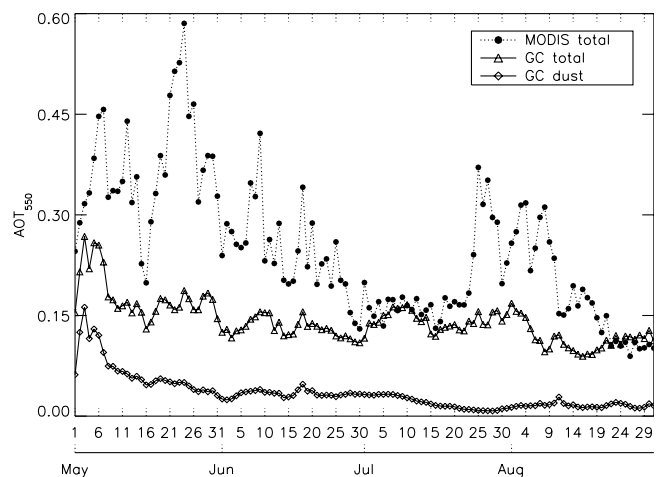


Figure 3. Daily total AOT₅₅₀ retrieved from MODIS observations (black dots), simulated with the GEOS-Chem model (open triangles), and simulated dust AOT₅₅₀ (open diamonds). For consistency with the rest of the study, we averaged the data over the region 40–70°N and 140–220°E (see the white box in Figure 2 and discussion in section 4).

Table 1. Monthly Biomass Burning Emissions for Carbonaceous Aerosols and CO in Russia [40–90°N; 60–180°E] From April to August 2003 and for the Entire Year 2003

Month of 2003	BC, Tg C	OC, Tg C	CO, Tg
April	0.01	0.15	1.45
May	0.07	0.76	9.86
June	0.05	0.6	8.48
July	0.13	1.46	19.44
August	0.03	0.42	7.54
Total in 2003	0.32	3.76	52.68

first two weeks, and decreases during the following months to become negligible in July and August. Therefore the fine fraction of dust likely only affects the simulated fine aerosol optical thickness in May and June.

[21] We thus hypothesize that the discrepancies between model results and satellite observations are rather due to a poor description of processes related to boreal fires in the model. *Edwards et al.* [2004] showed that MODIS AOT_f and MOPITT CO column are best correlated over regions influenced by biomass burning because of collocation of sources for the two species. They found that this correlation increases from very low ($r = 0.16$) to high ($r = 0.74$) in case of severe fire activity. In the present study, we found POLDER and MODIS AOT_f to be correlated with MOPITT CO column by $r = 0.59$ and $r = 0.58$, respectively, for the May–June–July–August (MJJJA) 2003 seasonal means, indicating that the North Pacific region is under a strong influence of boreal fires during that period.

4. Model Sensitivity to Processes Influencing the Aerosol and CO Distributions Over the North Pacific From May to August 2003

[22] In this section, we investigate the influence of the strength, the time resolution and the vertical distribution of biomass burning emissions, and deposition processes on the export of both aerosols and CO over the North Pacific ocean. We focus our analysis on the [40–70°N; 140–220°E] window (white box in Figure 2, top left) that is particularly influenced by the outflow from the boreal fires. In the following, we refer to that region as the “NPac” (North Pacific) window. Seasonal variations of the Asian outflow to the Pacific are typically driven by the two monsoon regimes [e.g., *Bey et al.*, 2001b; *Liu et al.*, 2003]. The conditions of spring and summer 2003 are close to these typical conditions. In the free troposphere, air masses north of 40°N, in particular over the Russian biomass burning sources, are transported southeast toward the Pacific and reach the NPac window. Air masses over China (south of 40°N) are transported northeastward, heading to the Pacific and can reach the NPac window. These meteorological conditions are similar in the upper troposphere.

4.1. Sensitivity to Biomass Burning Emissions: Strength and Temporal Resolution

[23] In April–May 2003 the fires were located in the southeastern part of Russia, bordering China and Mongolia (around Lake Baikal), and then moved northward to Siberia where fires occurred in July–August. Our model emission ratios CO/OC, CO/BC and BC/OC (derived from the yearly amounts in Table 1) are consistent with those

published by *Andreae and Merlet* [2001] for extratropical forests within 20%, 13% and 33%, respectively. In our standard scenario, the maximum of emissions occurs in July consistently with the maximum of active fires detected by the AATSR sensor (see section 2.3 and Table 1). The temporal distribution of fire emissions in Russia derived from MODIS and Advanced Very High Resolution Radiometer (AVHRR) by *Kasichke et al.* [2005] differs in that the maximum occurs in May 2003. This is likely due to the use of different satellite fire products (those from the AATSR are possibly subject to bias [*Kasichke et al.*, 2003]), and different assumptions used to derive emission amounts from different burned area inventories. *Damoah et al.* [2004] estimated that 24.75 Tg of CO were released by the Russian fires between 10 and 31 May (assuming 5.5×10^6 ha area burned as given by the Global Fire Monitoring Center (<http://www.fire.uni-freiburg.de/>) and a CO release of 4500 kg per hectare burned), which is more than twice our estimate for that month. Our annual biomass burning emissions for CO in 2003 (52.68 Tg) are in the low range of the estimates given by *Kasichke et al.* [2005] (55–139 Tg) and lower than those of *Jaffe et al.* [2004] (68 Tg) by 30%. We performed two sensitivity tests in which our trace gas and aerosol biomass burning emissions were increased by a factor of 1.5 (simulation *a*) and 3 (simulation *b*). The CO emissions in simulation *a* are consistent with the estimate by *Jaffe et al.* [2004] over the entire season, while in the simulation *b* the CO emissions are 30 Tg in May 2003, which is consistent with the estimate of *Damoah et al.* [2004] and *Yurganov et al.* [2005]. In a third sensitivity simulation *c*, we implemented a daily emission inventory for Russia by scaling the standard monthly emission amounts (Table 1) to a daily distribution of fires obtained using a 5-day running mean of the number of active fires detected by AATSR (Figure 4). The 5-day criteria was chosen to allow a complete coverage of the Earth surface by the satellite and to avoid a too high sensitivity to cloud cover.

[24] Regionally averaged daily CO, AOT_{f,865} and AOT_{f,550} columns obtained from the different sensitivity simulations are compared to satellite observations in Figure 5. The correlation and bias between model results and observations are presented in Tables 2 and 3 for the

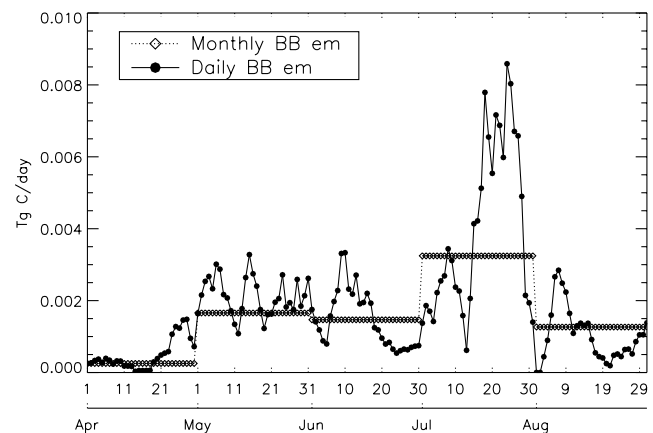


Figure 4. BC biomass burning emissions from April to August 2003. The daily inventory is shown with black dots while the monthly mean is shown with open diamonds.

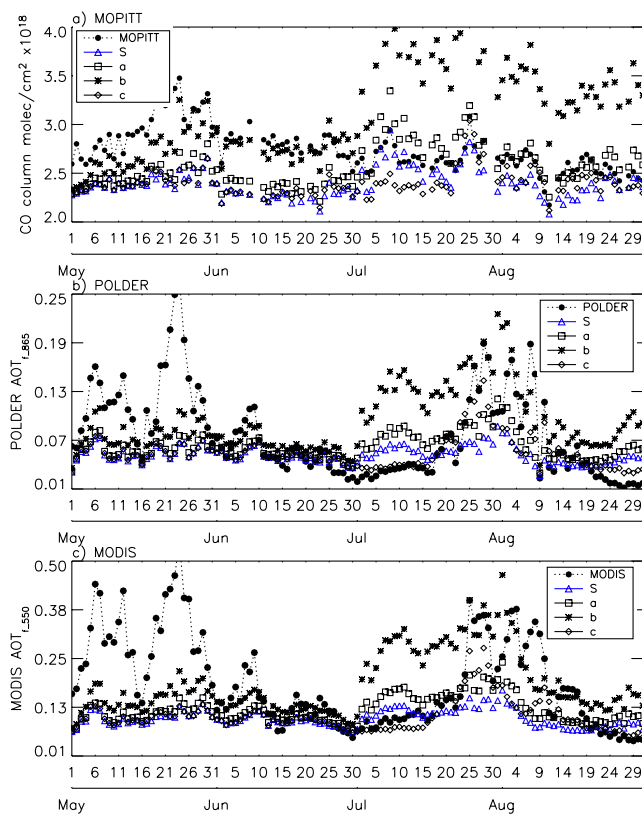


Figure 5. (a) Daily CO columns averaged within 40–70°N and 140–220°E (white box in Figure 2) retrieved from MOPITT observations (black dots) and simulated with the GEOS-Chem model. Triangles indicate standard model, squares indicate simulation *a*, stars indicate simulation *b*, and diamonds indicate simulation *c*. (b) Same for daily $AOT_{f_{865}}$. Observations are from POLDER. (c) Same for daily $AOT_{f_{550}}$. Observations are from MODIS. See Table 2 for description of the simulations.

May–June and July–August period, respectively. Figure 5 and Table 2 show that in May and June, simulations *a* and *c* do not agree significantly better than the standard simulation with the observations. Only the scenario including a factor of 3 in the biomass burning emissions

(simulation *b*) yields some improvements in May and June (correlations between the simulated and the observed aerosol optical thickness are increased from $r = 0.55$ to $r = 0.72$ for $AOT_{f_{865}}$ and from $r = 0.61$ to $r = 0.75$ for $AOT_{f_{550}}$). Note that the amplitude of peaks is still not well reproduced and the biases remain significant ($b = -22.4\%$ for $AOT_{f_{865}}$ and $b = -35.8\%$ for $AOT_{f_{550}}$). Simulation *b* does not modify significantly the correlation between simulated and observed CO but the bias is reduced by 71%. In July and August, an increase by a factor 3 in the biomass burning emissions leads to a significant overestimate of both the CO and aerosol columns in the NPac window. In July, this remains true also for simulation *a* but to a lower extent.

[25] Using biomass burning inventory resolved on a daily basis (simulation *c*) has no significant impact on the CO simulation (the correlation is even reduced in July–August) (Table 2). This result obtained for boreal regions is in agreement with those obtained by *Heald et al.* [2003a] for the Asian tropical regions. CO has a lifetime of several months and the continental boundary layer is well mixed within a few hours, which results in smoothing the local influence of the biomass burning CO emissions and can explain in part the relatively small differences between simulations using daily versus monthly inventories. *Heald et al.* [2003a] pointed out also an inadequate resolution of the model transport that can limit the advantage to be gained from fine temporal resolution of emissions. *Hyer et al.* [2007] found that in boreal regions, CO distributions are better reproduced by simulations using daily (rather than monthly) emission inventories, only for regions close to the sources as the signal induced by high-frequency emissions decrease rapidly with distance from the source. We find on the other hand that using a daily emission inventory increases significantly the correlation between the simulated aerosol optical thickness and the two satellite products (from $r = 0.52$ to $r = 0.84$ for $AOT_{f_{865}}$, and from $r = 0.45$ to $r = 0.81$ for $AOT_{f_{550}}$) and reduces the bias (by 37% for $AOT_{f_{865}}$ and 16% for $AOT_{f_{550}}$) (see also Table 3). Although a bias remains in comparison to MODIS, the POLDER satellite observations are particularly well

Table 2. Correlation (r) and Percent Bias^a (b) Calculated Between the Daily Simulated and Observed Data Averaged Over 40–70°N and 140–220°E for May–June 2003^b

Simulation		CO		$AOT_{f_{865}}$		$AOT_{f_{550}}$	
Label	Description	r	b	r	b	r	b
S	standard	0.70	−18.7	0.55	−42.4	0.61	−54.6
a	BB emission $\times 1.5$	0.77	−15.4	0.62	−37.4	0.67	−50.0
b	BB emission $\times 3$	0.65	−5.4	0.72	−22.4	0.75	−35.8
c	BB emission daily	0.72	−18.1	0.55	−41.2	0.65	−53.4
d	EIH up to 3 km	0.70	−18.6	0.60	−39.6	0.65	−52.1
e	EIH up to 4.5 km	0.70	−18.5	0.60	−37.3	0.64	−50.0
f	EIH up to 6.5 km	0.65	−18.0	0.57	−33.8	0.62	−46.5
g	e-folding time = 2	0.70	−18.5	0.54	−41.7	0.60	−54.0
h	no scavenging	0.71	−17.9	0.21	−25.5	0.16	−40.4
i	no rainout/washout	0.73	−17.3	0.30	20.7	0.49	−0.3
BE	best estimate	0.82	−8.1	0.79	−26.3	0.83	−39.6

^aComputed as (model-observations)/observations.

^bObservations used are CO columns from MOPITT (first column), $AOT_{f_{865}}$ from POLDER (second column) and $AOT_{f_{550}}$ from MODIS (third column).

Table 3. Same as Table 2 but for July–August 2003

Simulation		CO		AOT _{f 865}		AOT _{f 550}	
Label	Description	r	b	r	b	r	b
S	standard	0.78	−6.1	0.52	−14.8	0.45	−33.3
a	BB emission × 1.5	0.78	3.9	0.56	9.3	0.49	−14.1
b	BB emission × 3	0.75	35.5	0.62	87.57	0.54	47.4
c	BB emission daily	0.63	−6.7	0.84	−9.3	0.81	−28.1
d	EIH up to 3 km	0.80	−4.4	0.62	1.7	0.54	−18.1
e	EIH up to 4.5 km	0.82	−4.9	0.68	10.2	0.60	−10.5
f	EIH up to 6.5 km	0.82	−2.0	0.73	20.5	0.69	−1.1
g	e-folding time = 2	0.78	−5.9	0.53	−13.4	0.45	−32.3
h	no scavenging	0.78	−4.3	0.61	30.0	0.54	3.6
i	no rainout/washout	0.78	−4.0	0.37	70.6	0.26	35.5
BE	best estimate	0.72	−1.8	0.92	12.4	0.90	−8.9

reproduced in July by the simulation *c* (Figures 5b and 5c). This indicates that using an aerosol inventory with a high temporal resolution can correct discrepancies between model and observations even if the total amount of emissions is kept constant. The timing of aerosol sources appears thus to be more important than that of CO, which is likely due to the larger sensitivity of aerosols to wet deposition.

4.2. Sensitivity to Emission Injection Heights

[26] Biomass burning emissions are distributed homogeneously within the PBL (which, according to our model, extends to 1.6 km height on average over the MJJA season in the fire region) in our standard simulation. Several studies suggest however that gases and particles emitted by fires can be injected at higher altitudes, in particular in the case of boreal forest fires. *Lavoué et al.* [2000] suggested emission injection heights (EIH) of 2300 m for Russian fires and up to 7600 m for Canadian fires that generally burn the tree crown. Recently *Fromm and Servranckx* [2003] and *Fromm et al.* [2005] documented episodes of particles from Canadian forest fires that were injected directly into the lower stratosphere. For the 2003 Russian boreal fires, a common assumption currently used in global models is to distribute fire emissions from the surface up to about 4 km [*Damoah et al.*, 2004; *Jaffe et al.*, 2004]. For the 2004 North American fires, *Turquety et al.* [2007] distributed also part of the emission in the upper troposphere (30% in between 400 and 200 hPa). We tested here three maximal injection altitudes at 3, 4.5 and 6.5 km (simulations *d*, *e* and *f*, respectively) and examine their impact on the CO and fine aerosol optical thickness distributions over the North Pacific during spring and summer 2003. The emissions over Russia are distributed from the surface up to the maximal level following the scheme presented in Figure 6 in the three cases (D. Lavoué, personal communication, 2006). Although the vertical distribution of the injection of fire products is not well known, we choose to inject most of them in the higher levels (i.e., 3, 4.5 and 6.5 km), an assumption which is consistent with the results of two recent studies [*Leung et al.*, 2007; *Turquety et al.*, 2007].

[27] The results are presented in Figure 7 (regionally averaged daily columns) and Tables 2 and 3 (statistics). In May and June 2003, none of the three scenarios modifies the standard simulation (Figure 7). In contrast, in July and August, the bias between model and observations (especially for aerosols) are reduced and the correlations

are improved in all three simulations *d*, *e* and *f* (Table 3). However, the simulations *e* and *f* (i.e., with the highest EIH) tend to overestimate the aerosol columns in early July in the NPac window. In late July and August, some maxima observed in the NPac window can be better reproduced by the simulation *f*. For instance, the peak between 30 July and 4 August (Figures 7b and 7c) is better reproduced in terms of amplitude but also in terms of phasing (the maximum occurs on 1 August in the standard simulation while it occurs on 3–4 August in simulation *f* consistently with the observations (Figure 7c)). According to *Kasischke et al.* [2005], surface fires are generally prevalent in the spring while the occurrence of crown fires increases in summer (or late fire season) because of different temperature, relative humidity, precipitation and fuel moisture content conditions. Although crown fires are believed to be less abundant in the Russian boreal forest than in North America [*Kasischke et al.*, 2005], some have already been documented during large fire years such as 1998 [*Kasischke and Bruhwiler*, 2002]. Our results suggest that the improved model CO and aerosol columns (simulations *e* and *f*) in July

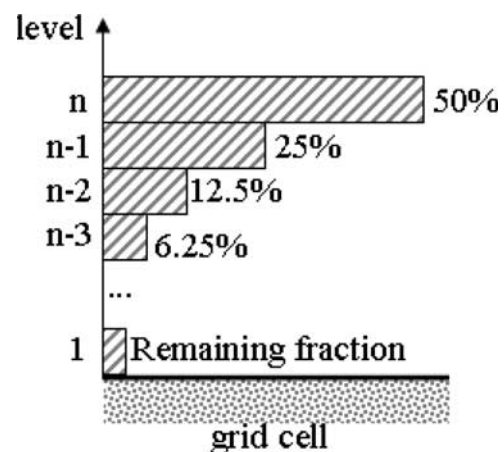


Figure 6. Vertical distribution of the Russian fire emissions used in simulations *d*, *e* and *f*. *n* corresponds to the maximum level at which emissions are injected. 50% of the emissions are injected at that level, half of the remaining fraction (i.e., 25%) is injected in the level below, and so on, until the first level (D. Lavoué, personal communication, 2006). Three maximum injection height are tested (3, 4.5 and 6.5 km).

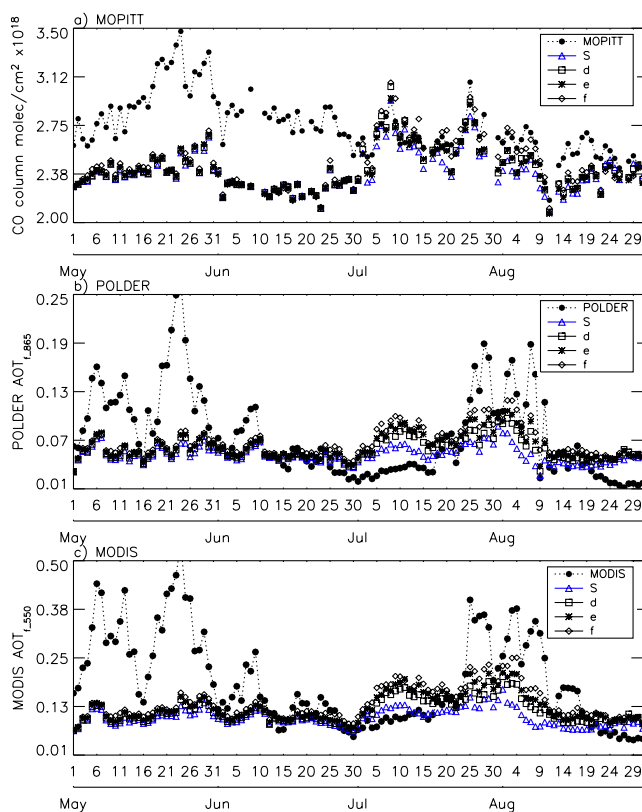


Figure 7. Same as Figure 5 but for simulations *d* (squares), *e* (stars) and *f* (diamonds).

and August reflect a better representation of the crown fires that are typical of the late fire season.

4.3. Sensitivity to Aerosol Deposition

[28] Overall, for the region and period investigated here, the standard model reproduces better the CO columns than the fine aerosol optical thickness (Figure 2). One major difference between aerosols and CO is that only the former experiences deposition. Wet removal being dominant for the fine mode particles, we tested the sensitivity of the model to the processes involved in aerosol wet deposition. A parameter, which can substantially influence the aerosol wet deposition, is the conversion of carbonaceous aerosols from hydrophobic to hydrophilic state, parameterized in the standard model with an e-folding time of 1.15 days. We increased this standard value to 2 days (simulation *g*) and to 5 days (not shown). No significant modifications of the aerosol and CO columns were seen within the NPac window (Figure S2 of the auxiliary material and Tables 2 and 3), which is in agreement with the study of *Park et al.* [2005]. In one sensitivity simulation *h*, we turned off the aerosol loss in convective updrafts (which is function of the scavenging efficiency) for primary carbonaceous and sulphate-nitrate-ammonium aerosols. This results in an increase of the discrepancies between simulated and observed aerosol columns in May and June. The amplitudes of the observations are not reproduced and the correlations with the satellite aerosol products are significantly decreased (Figure S2 of the auxiliary material and Tables 2 and 3). We also performed a simulation *i* in which the rainout

(in-cloud scavenging) and washout (below-cloud scavenging) processes were turned off in the region of fires. The results (Figure S2 of the auxiliary material and Tables 2 and 3) indicate (as expected) a high overestimate of the simulated fine aerosol optical thickness compared to the observations. In summary, suppressing or decreasing deposition results in a significant decrease of the correlations between model and observations, which indicates that the occurrence of the wet deposition events (e.g., rain) is likely to be reasonably reproduced by the model. No data are available to further evaluate the simulated deposited amount.

4.4. “Best Estimate” Scenario

[29] On the basis of the results presented above (see also Figure S3 of the auxiliary material) and on additional tests (not presented here) in which different processes were assembled in various configurations (e.g., using daily biomass burning emission inventories and increasing their total amount by a factor 1.5), we concluded that the model best represents the outflow associated with the 2003 Russian fires with the following setup: (1) daily biomass burning emission inventories, (2) EIH up to 4.5 km in July and August, and (3) biomass burning emission amounts in May increased by a factor 3. We will hereafter refer to that case as our “best estimate” (BE) simulation. As discussed in the previous sections, the increase in biomass burning emission by a factor 3 in May could be attributed either to a shortcoming in

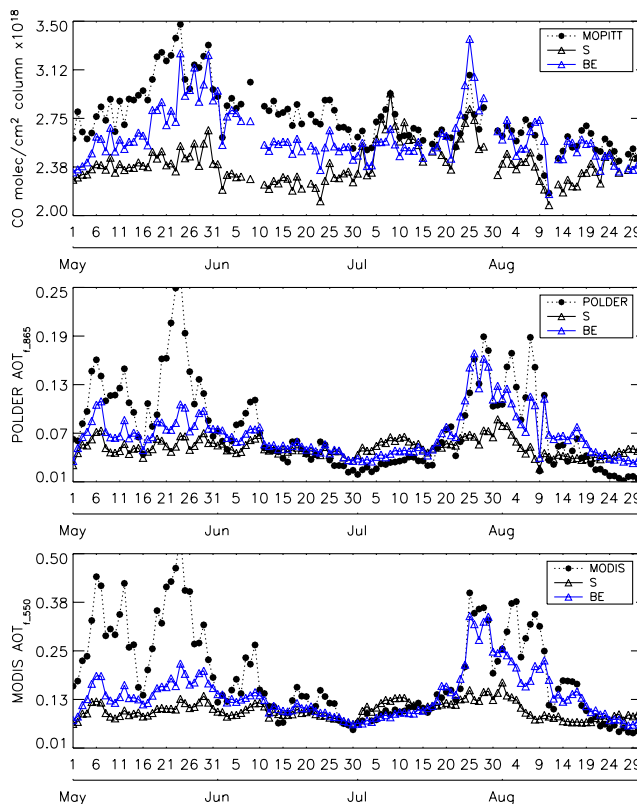


Figure 8. Daily CO columns, $AOT_{f_{865}}$ and $AOT_{f_{550}}$ retrieved from satellite observations (black dots) and simulated with the GEOS-Chem model (standard (black triangles) and BE (blue triangles) simulations), averaged within 40–70°N and 140–220°E (white box in Figure 2).

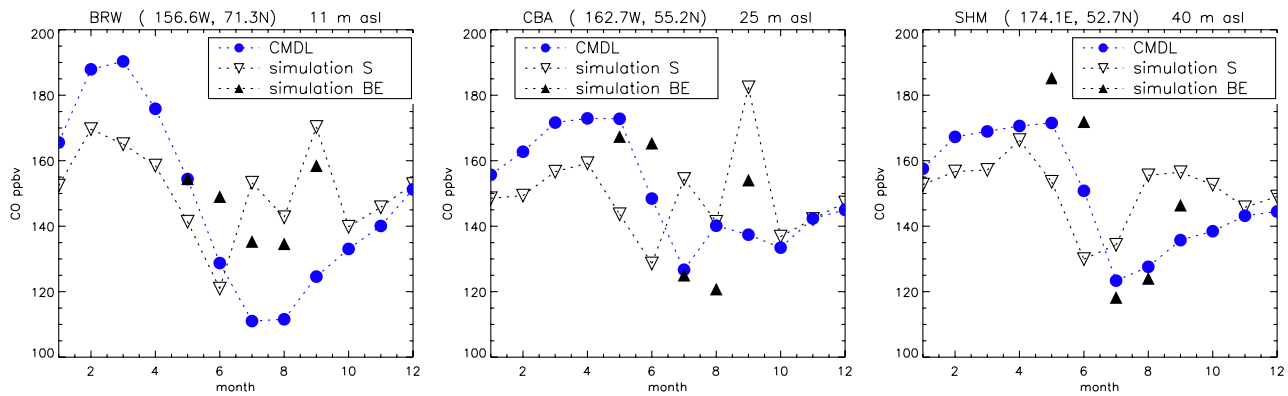


Figure 9. Monthly mean surface CO concentrations from in situ measurements (CMDL) (black dots), from the standard simulation (open triangles), and from the BE simulation (black triangles) from May to September 2003 at three sites.

the active fire data set used to constrain the temporal variations in the emission inventories (section 4.1) or, for CO, to an underestimate of the background concentrations (section 3). EIH up to 4.5 km in the late fire season are consistent with increased severity of the fires induced by dryer conditions and vegetation growth (section 4.2).

[30] Figure 8 presents the daily CO columns, $AOT_{f,865}$ and $AOT_{f,550}$ resulting from this BE simulation and Tables 2 and 3 provide the relevant statistics. The BE simulation greatly improves upon the standard simulation for both CO and aerosols. Some discrepancies remain in terms of amplitudes for the aerosol simulation especially in May and June, but part of this disagreement may be due to the fine dust component as discussed in section 3. The validity of our BE simulation is further confirmed by comparisons of the simulated surface CO concentrations with measurements made available via the NOAA/CMDL network (<http://www.cmdl.noaa.gov/infodata/ftpdata.html>) (Figure 9). For comparisons to those measurements, we extended the BE

simulation to September 2003 using the standard scenario (assuming no Russian fires at that period). Three sites are particularly well suited for the evaluation of our simulations because of their location (see Figure 2) and of the large temporal cover in 2003. The two sites in the North Pacific (“SHM” and “CBA”) confirm that the BE simulation provides some improvements in the simulation of surface CO compared to the standard simulation. The site in Alaska (Barrow, “BRW”) is better simulated in terms of temporal variation, but the July and August CO concentrations remain overestimated. Unfortunately, no aerosol observations are available to further evaluate our BE simulation.

[31] Figure 10 presents the ratio between CO mixing ratios at 250 hPa and those at 700 hPa (referred to as R_{vert}) for May and August 2003, which provides some indications on the vertical CO distributions [Edwards *et al.*, 2006]. R_{vert} from the BE simulation agrees better with MOPITT than that of the standard scenario (the correlation is increased from $r = 0.4$ to $r = 0.5$ on average over the whole region

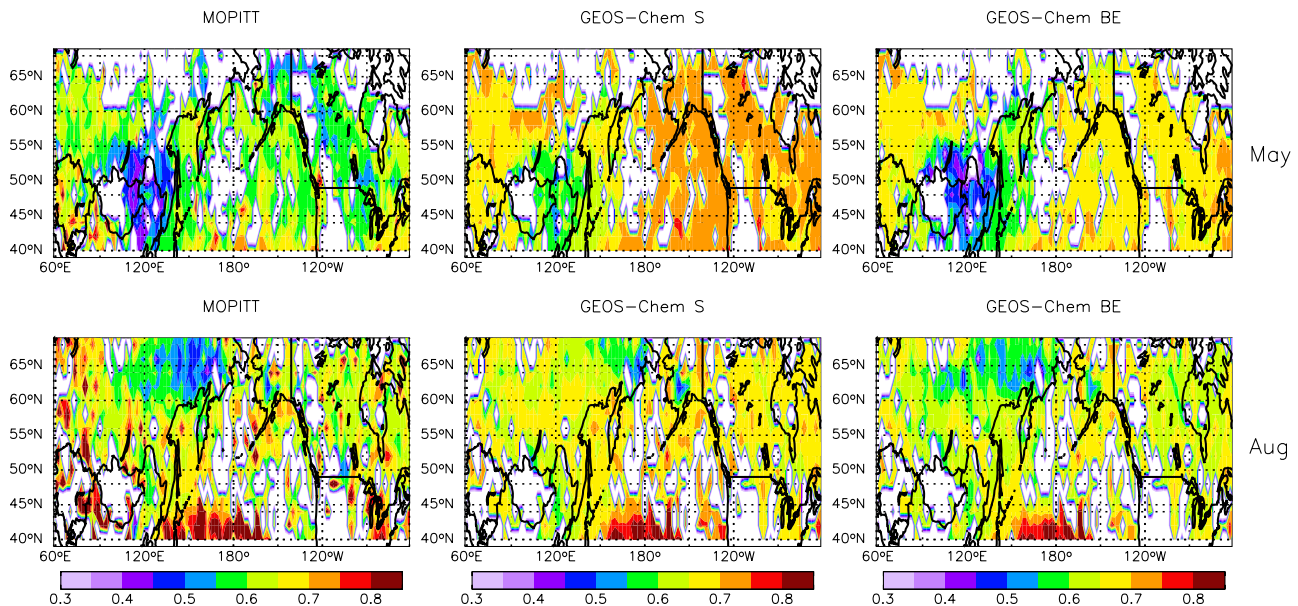


Figure 10. Mean monthly ratios of MOPITT CO mixing ratios between 250 and 700 hPa for May and August 2003. No data are shown for cloudy pixels or for background conditions where the CO mixing ratios is less than 100 ppbv at both levels (in order to sample only recent plumes).

shown in Figure 10 for both months). In May, the standard simulation overestimates R_{vert} in the Russian biomass burning source region and in the “nearby” Pacific ocean, as well as in the eastern part of the Pacific (“remote”) and over the United States compared to the MOPITT data. These discrepancies are well corrected by the BE simulation in the source regions and nearby, and partially corrected in the remote regions. This reflects an underestimate of the CO concentrations transported in the lower layers in the standard simulation. In August, differences between the BE and the standard simulation are mainly located over the Siberian biomass burning source region (north of 55°N), indicating that the assumptions used to inject particles at higher altitudes better reproduce the observations.

5. Impacts of the 2003 Russian Fires on the Arctic Aerosol Composition

[32] In this section, we quantify the impact of the 2003 Russian fires in terms of atmospheric aerosol burden via their contributions to the fine aerosol thickness north

of 75°N and in terms of BC deposition over Arctic. For that purpose, we compare our BE simulation to a simulation with the Russian biomass burning emissions turned off. Differences between the BE and the standard simulations are also briefly highlighted.

5.1. AOT

[33] Table 4 gives the monthly mean $\text{AOT}_{\text{F}_{550}}$ averaged north of 75°N obtained from the standard and BE simulations for each month from May to August 2003. We also indicate the contribution of the 2003 Russian fires to the aerosol optical thickness north of 75°N (Table 4). The simulated $\text{AOT}_{\text{F}_{550}}$ are characteristic of spring and summer background values in the Arctic, e.g., in the high range of measurements provided by *Herber et al.* [2002] at Spitzbergen (Norway) for summer (0.046 ± 0.024 at 532 nm). Figure 11 shows that the Russian fires contribute mostly to the aerosol fine fraction over east Russia, the North Pacific and the North American Arctic in May (and June, not shown) and also over most of the regions north of 50°N in July (and August, not shown). They contribute up to 30%

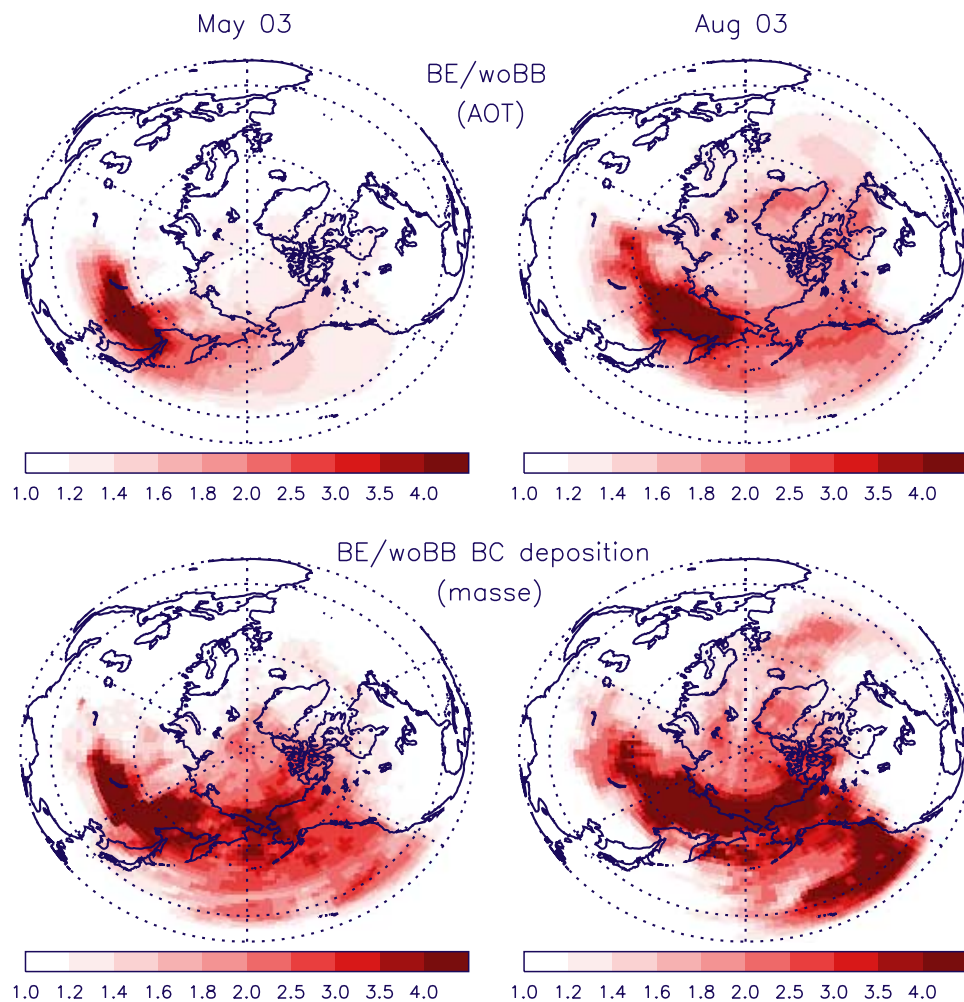


Figure 11. (top) Monthly mean $\text{AOT}_{\text{F}_{550}}$ ratio between the BE simulation and a simulation with Russian biomass burning emissions turned off (“BE/woBB”). (bottom) Monthly mean black carbon wet deposition ratio between the BE simulation and a simulation with Russian biomass burning emissions turned off for (left) May 2003 and (right) August 2003.

Table 4. Monthly Mean $AOT_{f,550}$ Averaged North of $75^{\circ}N$ as Given by the Standard and BE Simulations (“ $AOT_{f,550}$ S” and “ $AOT_{f,550}$ BE,” Respectively) and the Contribution of the 2003 Russian Fires to the AOT_f (“ AOT_{fires} ”) as Given by Our BE Simulations in Absolute Value and Percent (in Parentheses)^a

Month of 2003	$AOT_{f,550}$ S	$AOT_{f,550}$ BE	AOT_{fires} BE (%)
May	0.056	0.063	0.010 (16)
June	0.061	0.071	0.017 (24)
July	0.054	0.060	0.020 (33)
August	0.050	0.066	0.023 (35)

^aWe computed AOT_{fires} as the difference between the aerosol optical thickness in the BE simulation and that from a simulation with the Russian biomass burning sources turned off. The relative contribution is estimated as $AOT_{fires}/AOT_{f,550}$ BE.

to the Arctic aerosol optical thickness in July and August 2003 (Table 4). Figure 12 shows the number of days in the MJJA period for which the daily $AOT_{f,550}$ simulated by the BE is greater than 0.094 (a threshold used to define Arctic Haze events at 532 nm [e.g., Herber *et al.*, 2002]) as well as the mean relative contribution of the Russian fires to the aerosol optical thickness for those days. According to the BE simulation, the number of the so-called Arctic Haze episodes is larger in the Russian and Atlantic Arctic (east of 0°) than in the Canadian Arctic, the lowest number of pollution episodes occurring over Greenland. On the other hand, the contribution of the Russian fires is small in the Atlantic and west Russian area (between $20^{\circ}W$ and $90^{\circ}E$) and exceeds 25% in most of the east Russian and North American Arctic.

[34] Overall, the results of the BE simulation are significantly different than those of the standard simulation. Aerosol optical thickness are enhanced by up to a factor 2 in the BE simulation compared to the standard scenario (Figure S4 of the auxiliary material). In May 2003, the increase in the aerosol optical thickness (with respect to the standard simulations) is mostly localized over the source region (because of the increase of the biomass burning emission by a factor 3), while in August 2003, the increase

Table 5. Total Mass of BC Deposited per Month in $\mu g m^{-2}$ North of $75^{\circ}N$ as Given by the Standard and BE Simulations (“ BC_{tot} S” and “ BC_{tot} BE,” Respectively) and the Contribution of the 2003 Russian Fires to the Total Mass Deposited (“ BC_{fires} ”) as Given by the BE Simulation in Mass and Percent (in Parentheses)^a

Month of 2003	BC_{tot} S, $mg m^{-2}$	BC_{tot} BE, $mg m^{-2}$	BC_{fires} , $mg m^{-2}$ (%)
May	315	425	165 (39)
June	284	400	205 (51)
July	730	678	383 (56)
August	598	787	423 (54)

^aWe computed BC_{fires} as the difference between the mass deposited in the BE simulation and that from a simulation with the Russian biomass burning sources turned off. The relative contribution is estimated as BC_{fires}/BC_{tot} BE.

in aerosol optical thickness is seen over a larger region including the north Atlantic, Greenland, and the entire Arctic region. This reflects the influence of the higher injection height, as particles injected directly in the free troposphere are transported over greater distances (because of increased wind and reduced deposition).

5.2. BC Deposition

[35] Light-absorbing aerosols are known to reduce the snow albedo even when present in very small amount in the snow [Warren and Wiscombe, 1980; Clarke and Noone, 1985; Hansen and Nazarenko, 2003]. Recent studies have pointed out the possible contribution of boreal fire emissions to the subsequent radiative forcing [Kim *et al.*, 2005; Stohl *et al.*, 2006]. The 2003 Russian fires influenced the deposition of BC over the entire Arctic region during the four months analyzed in this study (Figure 11). In May and June, the deposition of BC is enhanced by a factor 1.8–2.5 because of the boreal fires. In July and August, the increase can reach up to a factor 4 in the Russian sector of the Arctic. Table 5 provides the total mass of BC deposited per month north of $75^{\circ}N$ as given by the standard and BE simulations. We also give the contribution of the Russian fires to the total

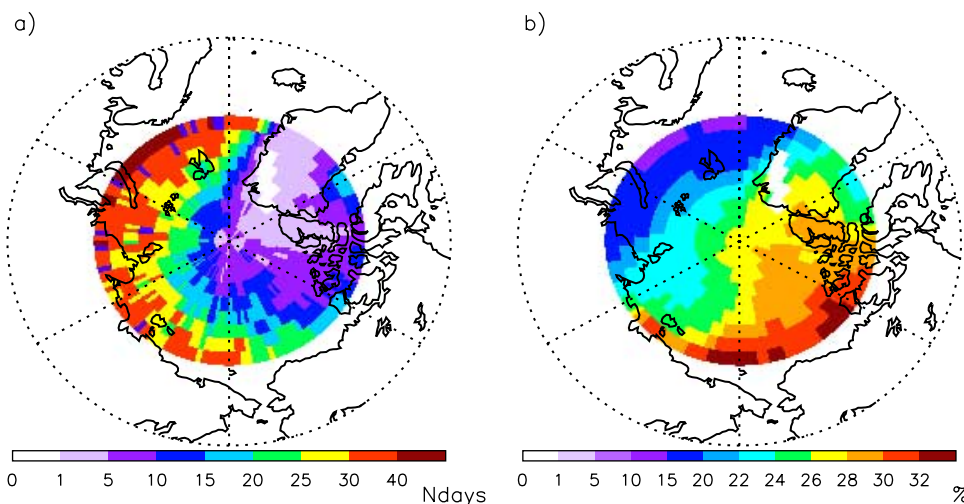


Figure 12. (a) Number of days (during the MJJA season) for which the $AOT_{f,550}$ of the fine aerosol fraction is greater than 0.094, a characteristic value for Arctic haze events [Herber *et al.*, 2002], and (b) contribution of the 2003 Russian fires to the AOT_f of those days in percent.

mass of BC deposited (Table 5). The contribution of the fires to the BC deposition ranges between 39% (May) and 56% (July). *Park et al.* [2005] estimated that the BC deposition flux north of 70°N is $58 \pm 12 \text{ Gg C yr}^{-1}$. The total deposition of BC (sum over the latitudes north of 70°N and over the months from May to August 2003) given by the BE simulation yields 25 Gg C, which is consistent with the value given by *Park et al.* [2005]. *Stohl et al.* [2006] argue that $130 \mu\text{g m}^{-2}$ can be a sufficient amount to impact snow albedo. Our estimates exceed $400 \mu\text{g m}^{-2}$ per month.

[36] As for the aerosol optical thickness, the May increase of the emissions results in an increase in the deposition (Figure S4 of the auxiliary material). However, the BE simulation does not necessarily lead to an increase in BC deposition in comparison to the standard simulation. In fact, the use of daily emission inventories and higher EIH result either in an increase or a decrease of the amount of BC that can experience wet deposition at each model time step (see for instance August 2003). The decrease in BC deposition in the BE simulation is mostly located over the source regions of Russia, consistently with the fact that particles are exported out of the continent more rapidly because of their higher initial altitudes. In July (not shown here), the decrease in BC deposition is even more pronounced and covers a large part of the Arctic region and the North Pacific east of 180°.

6. Summary and Conclusions

[37] In this study, we address the issues of the representation of boreal fires in a global chemistry and transport model as well as their role in the Arctic aerosol optical thickness and BC deposition. We focus on the severe 2003 Russian fires from May to August 2003. We use the GEOS-Chem model to conduct several sensitivity studies to evaluate how the strength, the time resolution, and the vertical distribution of biomass burning emissions as well as the deposition processes affect the long-range transport of aerosols and CO. We analyze several sensitivity simulations: three involving the Russian fire sources (increase of the biomass burning emission by factors 1.5 and 3, and use of a daily timescale for emissions); three involving the Russian fire emission injection height (up to 3, 4.5 and 6.5 km) and three in which we modify the deposition processes (suppressing scavenging, rainout and washout, and increasing the time of hydrophobic-hydrophilic particle conversion, respectively).

[38] In the standard configuration, the model significantly underestimates the MOPITT CO columns, POLDER and MODIS fine aerosol optical thickness over the North Pacific through May to August 2003. Although satellite products can suffer from large bias (e.g., difficulties in aerosol detection over land), we suggest that these discrepancies originate to a large extent from a misrepresentation of boreal fires in the model. Our initial 2003 Russian biomass burning sources tend to be underestimated compared to other studies. However, increasing the amount of CO and aerosols emitted does not necessarily results in significant improvements of our simulations (except in May 2003). In contrast, the use of daily biomass burning emission inventories (rather than monthly) generally improved the aerosol sim-

ulations, without any significant effect on the CO columns. The injection of particles above the planetary boundary layer also impacts our simulated CO and aerosol columns but only in the late fire season (July and August). This probably reflects a larger occurrence of crown fires in the late fire season and a restriction of surface fires to the beginning of the fire season. A large decrease in the aerosol deposition results in a significant decrease of the correlations between model and observations, which indicates that the occurrence of the wet deposition events is likely to be reasonably reproduced. We best reproduce the 2003 Russian fire export to the North Pacific using daily fire emission inventories and maximal injection of particles up to 4.5 km in the late fire season. In May, following the literature, we increased our emissions from 9.9 to 29.6 Tg of CO (and consistently for BC and OC) in order to correct a possible shortcoming of our satellite active fire data set from which the emissions are derived. A total of 72 Tg of CO, 0.5 Tg C of BC and 5.3 Tg C of OC are injected over the entire fire season in our best estimate simulation.

[39] Compared to the standard simulation, the BE model configuration results in an enhancement of the contribution of the Russian fires to distant locations and yield significant differences in aerosol optical thickness and BC deposition on the Arctic by up to a factor 2. The differences between the two model configurations provide an evaluation of the expected range of current uncertainties in terms of boreal fire representation. According to our best estimate simulation, the 2003 Russian fires contribute between 16% and 35% to the monthly aerosol optical thickness averaged north of 75°N. The contribution of the Russian fires during the days of Arctic haze events in spring and summer can reach up to more than 30% of the AOT_f. Their contribution to BC deposition is greater than 50% during the summer months.

[40] Large uncertainties remain in terms of fire emission estimates. Recent studies used fire radiative energy measured from space to derive smoke emission rates, which is a promising tool although uncertainties are still large [*Wooster et al.*, 2003, 2005; *Ichoku and Kaufman*, 2005; *Roberts et al.*, 2005]. In addition, there is still a lack of data concerning the vertical distribution of species, in particular the injection height issue. We used here the information contained in the MOPITT retrievals to evaluate the CO model vertical profile, but no data were available to evaluate the aerosol vertical profiles. Data from the Cloud-Aerosol Lidar and Infrared Pathfinder Satellite Observations (CALIPSO) mission, that is operational since spring 2006, will allow further investigation of this issue.

[41] **Acknowledgments.** The Swiss Agency for Development and Cooperation (SDC) is acknowledged for funding. The GEOS-Chem model is managed by the Atmospheric Chemistry Modeling group at Harvard University with support from the NASA Atmospheric Chemistry Modeling Analysis Program. The MODIS data used in this study were acquired as part of NASA's Earth Science Enterprise. The algorithms were developed by the MODIS Science Teams. The data were processed by the MODIS Adaptive Processing System (MODAPS) and are archived and distributed by the Goddard DAAC. The POLDER instrument is developed by the Centre National d'Etudes Spatiales (CNES) and was on board the ADEOS platform developed by National Space Agency of Japan (NASDA). We thank the NCAR MOPITT team for providing the MOPITT data and the Carbon Cycle Greenhouse Gases group of the CMDL/NOAA for access to the CO surface measurements used in this study. The authors gratefully

acknowledge David Lavoué for helpful discussions. J.-L. Attié acknowledges the financial support from CNES.

References

- Alexander, B., R. J. Park, D. J. Jacob, Q. B. Li, R. M. Yantosca, J. Savarino, C. C. W. Lee, and M. H. Thiemens (2005), Sulfate formation in sea-salt aerosols: Constraints from oxygen isotopes, *J. Geophys. Res.*, *110*, D10307, doi:10.1029/2004JD005659.
- Andreae, M. O., and P. Merlet (2001), Emission of trace gases and aerosols from biomass burning, *Global Biogeochem. Cycles*, *15*, 955–966.
- Arctic Climate Impact Assessment (2004), *Impacts of a Warming Arctic: Arctic Climate Impact Assessment*, 146 pp., Cambridge Univ. Press, New York.
- Arino, O., and J. M. Melinotte (1995), *Fire Index Atlas, Earth Obs. Q.*, *50*, 11–16.
- Balkanski, Y. J., et al. (1993), Transport and residence times of tropospheric aerosols inferred from a global three-dimensional simulation of 210Pb, *J. Geophys. Res.*, *98*, 20,573–20,586.
- Benkovitz, C. M., et al. (1996), Global gridded inventories for anthropogenic emissions of sulfur and nitrogen, *J. Geophys. Res.*, *101*, 29,239–29,253.
- Bertschi, I. T., and D. A. Jaffe (2005), Long-range transport of ozone, carbon monoxide, and aerosols to the NE Pacific troposphere during the summer of 2003: Observations of smoke plumes from Asian boreal fires, *J. Geophys. Res.*, *110*, D05303, doi:10.1029/2004JD005135.
- Bey, I., et al. (2001a), Global modeling of tropospheric chemistry with assimilated meteorology: Model description and evaluation, *J. Geophys. Res.*, *106*, 23,073–23,095.
- Bey, I., et al. (2001b), Asian chemical outflow to the Pacific in spring: Origins, pathways, and budgets, *J. Geophys. Res.*, *106*, 23,097–23,113.
- Bond, T. C., D. G. Streets, K. F. Yarber, S. M. Nelson, J.-H. Woo, and Z. Klimont (2004), A technology-based global inventory of black and organic carbon emissions from combustion, *J. Geophys. Res.*, *109*, D14203, doi:10.1029/2003JD003697.
- Chin, M., et al. (2002), Tropospheric aerosols optical thickness from the GOCART model and comparisons with satellite and Sun photometer measurements, *J. Atmos. Sci.*, *59*, 461–483.
- Chu, D. A., Y. J. Kaufman, C. Ichoku, L. A. Remer, D. Tanré, and B. N. Holben (2002), Validation of MODIS aerosol optical depth retrieval over land, *Geophys. Res. Lett.*, *29*(12), 8007, doi:10.1029/2001GL013205.
- Chung, S. H., and J. H. Seinfeld (2002), Global distribution and climate forcing of carbonaceous aerosols, *J. Geophys. Res.*, *107*(D19), 4407, doi:10.1029/2001JD001397.
- Clarke, A. D., and J. Noone (1985), Measurements of soot aerosol in Arctic snow, *Atmos. Environ.*, *19*, 2045–2054.
- Cooke, W. F., et al. (1999), Construction of a $1^\circ \times 1^\circ$ degree fossil fuel emission data set for carbonaceous aerosol and implementation and radiative impact in the ECHAM4 model, *J. Geophys. Res.*, *104*, 22,137–22,162.
- Damoah, R., et al. (2004), Around the world in 17 days—Hemispheric-scale transport of forest fire smoke from Russia in May 2005, *Atmos. Chem. Phys.*, *4*, 1311–1321.
- Deeter, M. N., et al. (2003), Operational carbon monoxide retrieval algorithm and selected results for the MOPITT instrument, *J. Geophys. Res.*, *108*(D14), 4399, doi:10.1029/2002JD003186.
- Deeter, M. N., L. K. Emmons, D. P. Edwards, J. C. Gille, and J. R. Drummond (2004), Vertical resolution and information content of CO profiles retrieved by MOPITT, *Geophys. Res. Lett.*, *31*, L15112, doi:10.1029/2004GL020235.
- Deschamps, P.-Y., et al. (1994), The POLDER mission: Instrument characteristics and scientific objectives, *IEEE Trans. Geosci. Remote Sens.*, *32*, 598–615.
- Deuzé, J. L., et al. (2000), Estimate of the aerosol properties over the ocean with POLDER, *J. Geophys. Res.*, *105*, 15,329–15,346.
- Deuzé, J. L., et al. (2001), Remote sensing of aerosols over land surfaces from POLDER-ADEOS-1 polarized measurements, *J. Geophys. Res.*, *106*, 4913–4926.
- Duncan, B. N., R. V. Martin, A. C. Staudt, R. Yevich, and J. A. Logan (2003), Interannual and seasonal variability of biomass burning emissions constrained by satellite observations, *J. Geophys. Res.*, *108*(D2), 4100, doi:10.1029/2002JD002378.
- Edwards, D. P., et al. (2004), Observations of carbon monoxide and aerosols from the Terra satellite: Northern Hemisphere variability, *J. Geophys. Res.*, *109*, D24202, doi:10.1029/2004JD004727.
- Edwards, D. P., et al. (2006), Satellite-observed pollution from Southern Hemisphere biomass burning, *J. Geophys. Res.*, *111*, D14312, doi:10.1029/2005JD006655.
- Emmons, L. K., et al. (2004), Validation of Measurements of Pollution in the Troposphere (MOPITT) CO retrievals with aircraft in situ profiles, *J. Geophys. Res.*, *109*, D03309, doi:10.1029/2003JD004101.
- Flannigan, M. D., et al. (2000), Climate change and forest fires, *Sci. Total Environ.*, *262*, 221–229.
- Flannigan, M. D., et al. (2005), Future area burned in Canada, *Clim. Change*, *72*, 1–16.
- Fromm, M. D., and R. Servranckx (2003), Transport of forest fire smoke above the tropopause by supercell convection, *Geophys. Res. Lett.*, *30*(10), 1542, doi:10.1029/2002GL016820.
- Fromm, M., R. Bevilacqua, R. Servranckx, J. Rosen, J. P. Thayer, J. Herman, and D. Larko (2005), Pyro-cumulonimbus injection of smoke to the stratosphere: Observations and impact of a super blowup in northwestern Canada on 3–4 August 1998, *J. Geophys. Res.*, *110*, D08205, doi:10.1029/2004JD005350.
- Generoso, S., et al. (2003), Improving the seasonal cycle and interannual variations of biomass burning aerosol sources, *Atmos. Chem. Phys.*, *3*, 1211–1222.
- Generoso, S., et al. (2007), Assimilation of POLDER aerosol optical thickness into the LMDz-INCA model: Implications for the Arctic aerosol burden, *J. Geophys. Res.*, *112*, D02311, doi:10.1029/2005JD006954.
- Gérard, B., J.-L. Deuzé, M. Herman, Y. J. Kaufman, P. Lallart, C. Oudard, L. A. Remer, B. Roger, B. Six, and D. Tanré (2005), Comparisons between POLDER 2 and MODIS/Terra aerosol retrievals over ocean, *J. Geophys. Res.*, *110*, D24211, doi:10.1029/2005JD006218.
- Gillet, N. P., A. J. Weaver, F. W. Zwiers, and M. D. Flannigan (2004), Detecting the effect of climate change on Canadian forest fires, *Geophys. Res. Lett.*, *31*, L18211, doi:10.1029/2004GL020876.
- Goloub, P., et al. (1999), Validation of the first algorithm applied for deriving the aerosol properties over the ocean using the POLDER/ADEOS measurements, *IEEE Trans. Geosci. Remote Sens.*, *37*, 1586–1596.
- Hansen, J., and L. Nazarenko (2003), Soot climate forcing via snow and ice albedos, *Proc. Natl. Acad. Sci. U.S.A.*, *101*, 423–428, doi:10.1073/pnas.2237157100.
- Heald, C. L., D. J. Jacob, P. I. Palmer, M. J. Evans, G. W. Sachse, H. B. Singh, and D. R. Blake (2003a), Biomass burning emission inventory with daily resolution: Application to aircraft observations of Asian outflow, *J. Geophys. Res.*, *108*(D21), 8811, doi:10.1029/2002JD003082.
- Heald, C. L., et al. (2003b), Asian outflow and trans-Pacific transport of carbon monoxide and ozone pollution: An integrated satellite, aircraft, and model perspective, *J. Geophys. Res.*, *108*(D24), 4804, doi:10.1029/2003JD003507.
- Heald, C. L., D. J. Jacob, D. B. A. Jones, P. I. Palmer, J. A. Logan, D. G. Streets, G. W. Sachse, J. C. Gille, R. N. Hoffman, and T. Nehrkorn (2004), Comparative inverse analysis of satellite (MOPITT) and aircraft (TRACE-P) observations to estimate Asian sources of carbon monoxide, *J. Geophys. Res.*, *109*, D23306, doi:10.1029/2004JD005185.
- Heald, C. L., D. J. Jacob, R. J. Park, L. M. Russell, B. J. Huebert, J. H. Seinfeld, H. Liao, and R. J. Weber (2005), A large organic aerosol source in the free troposphere missing from current models, *Geophys. Res. Lett.*, *32*, L18809, doi:10.1029/2005GL023831.
- Herber, A., L. W. Thomason, H. Gernandt, U. Leiterer, D. Nagel, K. Schulz, J. Kaptur, T. Albrecht, and J. Notholt (2002), Continuous day and night aerosol optical depth observations in the Arctic between 1991 and 1999, *J. Geophys. Res.*, *107*(D10), 4097, doi:10.1029/2001JD000536.
- Herman, M., J.-L. Deuzé, A. Marchand, B. Roger, and P. Lallart (2005), Aerosol remote sensing from POLDER/ADEOS over the ocean: Improved retrieval using a nonspherical particle model, *J. Geophys. Res.*, *110*, D10S02, doi:10.1029/2004JD004798.
- Hoelzelmann, J. J., M. G. Schultz, G. P. Brasseur, C. Granier, and M. Simon (2004), Global Wildland Fire Emission Model (GWEM): Evaluating the use of global area burnt satellite data, *J. Geophys. Res.*, *109*, D14S04, doi:10.1029/2003JD003666.
- Hyer, E. J., E. S. Kasichke, and D. J. Allen (2007), Effects of source temporal resolution on transport simulations of boreal fire emissions, *J. Geophys. Res.*, *112*, D01302, doi:10.1029/2006JD007234.
- Ichoku, C., and Y. J. Kaufman (2005), A method to derive smoke emission rates from MODIS fire radiative energy measurements, *IEEE Trans. Geosci. Remote Sens.*, *43*, 2636–2649.
- Ito, A., and J. E. Penner (2005), Estimates of CO emissions from open biomass burning in southern Africa for the year 2000, *J. Geophys. Res.*, *110*, D19306, doi:10.1029/2004JD005347.
- Iziomon, M. G., U. Lohmann, and P. K. Quinn (2006), Summertime pollution events in the Arctic and potential implications, *J. Geophys. Res.*, *111*, D12206, doi:10.1029/2005JD006223.
- Jacob, D. J., J. H. Crawford, M. M. Kleb, V. S. Connors, R. J. Bendura, J. L. Raper, G. W. Sachse, J. C. Gille, L. Emmons, and C. L. Heald (2003), Transport and Chemical Evolution over the Pacific (TRACE-P)

- aircraft mission: Design, execution, and first results, *J. Geophys. Res.*, *108*(D20), 9000, doi:10.1029/2002JD003276.
- Jaffe, D., I. Bertsch, L. Jaeglé, P. Novelli, J. S. Reid, H. Tanimoto, R. Vingarzan, and D. L. Westphal (2004), Long-range transport of Siberian biomass burning emissions and impact on surface ozone in western North America, *Geophys. Res. Lett.*, *31*, L16106, doi:10.1029/2004GL020093.
- Kaplan, J. O., and M. New (2006), Arctic climate change with a 2°C global warming: Timing, climate patterns and vegetation change, *Clim. Change*, *79*, 213–241, doi:10.1007/s10584-006-9113-7.
- Kasischke, E. S., and L. P. Bruhwiler (2002), Emissions of carbon dioxide, carbon monoxide, and methane from boreal forest fires in 1998, *J. Geophys. Res.*, *107*, 8146, doi:10.1029/2001JD000461 [108(D1), 2003].
- Kasischke, E. S., and J. E. Penner (2004), Improving global estimates of atmospheric emissions from biomass burning, *J. Geophys. Res.*, *109*, D14S01, doi:10.1029/2004JD004972.
- Kasischke, E. S., J. H. Hewson, B. Stocks, G. van der Werf, and J. Randerson (2003), The use of ATSR active fire counts for estimating relative patterns of biomass burning – a study from the boreal forest region, *Geophys. Res. Lett.*, *30*(18), 1969, doi:10.1029/2003GL017859.
- Kasischke, E. S., E. J. Hyer, P. C. Novelli, L. P. Bruhwiler, N. H. F. French, A. I. Sukhinin, J. H. Hewson, and B. J. Stocks (2005), Influences of boreal fire emissions on Northern Hemisphere atmospheric carbon and carbon monoxide, *Global Biogeochem. Cycles*, *19*, GB1012, doi:10.1029/2004GB002300.
- Kaufman, Y. J., et al. (1997), Operational remote sensing of tropospheric aerosol over the land from EOS-MODIS, *J. Geophys. Res.*, *102*, 17,051–17,061.
- Kaufman, Y. J., et al. (2002), A satellite view of aerosols in the climate system, *Nature*, *419*, 215–222.
- Kim, Y., et al. (2005), Possible effect of boreal wildfire soot on Arctic sea ice and Alaska glaciers, *Atmos. Environ.*, *39*, 3513–3520.
- Koch, D., and J. Hansen (2005), Distant origins of Arctic black carbon: A Goddard Institute for Space Studies ModelE experiment, *J. Geophys. Res.*, *110*, D04204, doi:10.1029/2004JD005296.
- Köpke, P., et al. (1997), Global aerosol data set report, Max-Planck-Inst. für Meteorol., Hamburg, Germany.
- Langenfelds, R. L., R. J. Francey, B. C. Pak, L. P. Steele, J. Lloyd, C. M. Trudinger, and C. E. Allison (2002), Interannual growth rate variations of atmospheric CO₂ and its δ¹³C, H₂, CH₄, and CO between 1992 and 1999 linked to biomass burning, *Global Biogeochem. Cycles*, *16*(3), 1048, doi:10.1029/2001GB001466.
- Lavoué, D., et al. (2000), Modeling of carbonaceous particles emitted by boreal and temperate wildfires at northern latitudes, *J. Geophys. Res.*, *105*, 26,871–26,890.
- Leung, F.-Y. T., J. A. Logan, R. Park, E. Hyer, E. Kasischke, D. Streets, and L. Yurganov (2007), Impacts of enhanced biomass burning in the boreal forests in 1998 on tropospheric chemistry and the sensitivity of model results to the injection height of emissions, *J. Geophys. Res.*, *112*, D10313, doi:10.1029/2006JD008132.
- Liu, H., D. J. Jacob, I. Bey, and R. M. Yantosca (2001), Constraints from ²¹⁰Pb and ⁷Be on wet deposition and transport in a global three-dimensional chemical tracer model driven by assimilated meteorological fields, *J. Geophys. Res.*, *106*(D11), 12,109–12,128.
- Liu, H., D. J. Jacob, I. Bey, R. M. Yantosca, B. N. Duncan, and G. W. Sachse (2003), Transport pathways for Asian pollution outflow over the Pacific: Interannual and seasonal variations, *J. Geophys. Res.*, *108*(D20), 8786, doi:10.1029/2002JD003102.
- Lobert, J. M., W. C. Keene, J. A. Logan, and R. Yevich (1999), Global chlorine emissions from biomass burning: Reactive Chlorine Emission Inventory, *J. Geophys. Res.*, *104*(D7), 8373–8390.
- Martin, R. V., D. J. Jacob, R. M. Yantosca, M. Chin, and P. Ginoux (2003), Global and regional decreases in tropospheric oxidants from photochemical effects of aerosols, *J. Geophys. Res.*, *108*(D3), 4097, doi:10.1029/2002JD002622.
- Mattis, I., A. Ansmann, U. Wandinger, and D. Müller (2003), Unexpectedly high aerosol load in the free troposphere over central Europe in spring/summer 2003, *Geophys. Res. Lett.*, *30*(22), 2178, doi:10.1029/2003GL018442.
- Müller, D., I. Mattis, U. Wandinger, A. Ansmann, D. Althausen, and A. Stohl (2005), Raman lidar observations of aged Siberian and Canadian forest fire smoke in the free troposphere over Germany in 2003: Microphysical particle characterization, *J. Geophys. Res.*, *110*, D17201, doi:10.1029/2004JD005756.
- Nedelec, P., V. Thouret, J. Brioude, B. Sauvage, J.-P. Cammas, and A. Stohl (2005), Extreme CO concentrations in the upper troposphere over north-east Asia in June 2003 from in situ MOZAIC aircraft data, *Geophys. Res. Lett.*, *32*, L14807, doi:10.1029/2005GL023141.
- Palmer, P. I., D. J. Jacob, D. B. A. Jones, C. L. Heald, R. M. Yantosca, J. A. Logan, G. W. Sachse, and D. G. Streets (2003), Inverting for emissions of carbon monoxide from Asia using aircraft observations over the western Pacific, *J. Geophys. Res.*, *108*(D21), 8828, doi:10.1029/2003JD003397.
- Park, R. J., D. J. Jacob, M. Chin, and R. V. Martin (2003), Sources of carbonaceous aerosols over the United States and implications for natural visibility, *J. Geophys. Res.*, *108*(D12), 4355, doi:10.1029/2002JD003190.
- Park, R. J., D. J. Jacob, B. D. Field, R. M. Yantosca, and M. Chin (2004), Natural and transboundary pollution influences on sulfate-nitrate-ammonium aerosols in the United States: Implications for policy, *J. Geophys. Res.*, *109*, D15204, doi:10.1029/2003JD004473.
- Park, R. J., et al. (2005), Export efficiency of black carbon aerosol in continental outflow: Global implications, *J. Geophys. Res.*, *110*, D11205, doi:10.1029/2004JD005432.
- Park, R. J., et al. (2006), Regional visibility statistics in the United States: Natural and transboundary pollution influences, and implications for the Regional Haze Rule, *Atmos. Environ.*, *40*, 5405–5423.
- Patterson, E. M., et al. (1977), Complex index of refraction between 300 and 700 nm for saharan aerosols, *J. Geophys. Res.*, *82*, 3153–3160.
- Randerson, J. T., et al. (2006), The impact of boreal forest fire on climate warming, *Science*, *314*, 130–132.
- Remer, L. A., et al. (2002), Validation of MODIS aerosol retrieval over ocean, *Geophys. Res. Lett.*, *29*(12), 8008, doi:10.1029/2001GL013204.
- Remer, L. A., et al. (2005), The MODIS aerosol algorithm, products, and validation, *J. Atmos. Sci.*, *62*, 947–973.
- Rinke, A., K. Dethloff, and M. Fortmann (2004), Regional climate effects of Arctic Haze, *Geophys. Res. Lett.*, *31*, L16202, doi:10.1029/2004GL020318.
- Roberts, G., M. J. Wooster, G. L. W. Perry, N. Drake, L.-M. Rebelo, and F. Dipotso (2005), Retrieval of biomass combustion rates and totals from fire radiative power observations: Application to southern Africa using geostationary SEVIRI imagery, *J. Geophys. Res.*, *110*, D21111, doi:10.1029/2005JD006018.
- Rodgers, C. D. (2000), *Inverse Method for Atmospheric Sounding: Theory and Practice*, World Sci., Hackensack, N. J.
- Schultz, M. G. (2002), On the use of ATSR fire count data to estimate the seasonal and interannual variability of vegetation fire emissions, *Atmos. Chem. Phys.*, *2*, 387–395.
- Shaw, G. E. (1995), The Arctic haze phenomenon, *Bull. Am. Meteorol. Soc.*, *76*, 2403–2412.
- Smirnov, A., et al. (2006), Ship-based aerosol optical depth measurements in the Atlantic Ocean: Comparison with satellite retrievals and GOCART model, *Geophys. Res. Lett.*, *33*, L14817, doi:10.1029/2006GL026051.
- Stohl, A. (2006), Characteristics of atmospheric transport into the Arctic troposphere, *J. Geophys. Res.*, *111*, D11306, doi:10.1029/2005JD006888.
- Stohl, A., et al. (2006), Pan-Arctic enhancements of light absorbing aerosol concentrations due to North American boreal forest fires during summer 2004, *J. Geophys. Res.*, *111*, D22214, doi:10.1029/2006JD007216.
- Streets, D. G., et al. (2003), An inventory of gaseous and primary aerosol emissions in Asia in the year 2000, *J. Geophys. Res.*, *108*(D21), 8809, doi:10.1029/2002JD003093.
- Tanré, D., et al. (1997), Remote sensing of aerosol properties over oceans using MODIS/EOS spectral radiances, *J. Geophys. Res.*, *102*, 16,971–16,988.
- Turquetly, S., et al. (2007), Inventory of boreal fire emissions for North America in 2004: Importance of peat burning and pyroconvective injection, *J. Geophys. Res.*, *112*, D12S03, doi:10.1029/2006JD007281.
- van der Werf, G., et al. (2003), Carbon emissions from fires in tropical and subtropical ecosystems, *Global Change Biol.*, *9*, 547–562.
- van der Werf, G. R., et al. (2004), Continental-scale partitioning of fire emissions during the 1997 to 2001 El Niño/La Niña period, *Science*, *303*, 73–76.
- Warren, S. G., and W. J. Wiscombe (1980), A model for the spectral albedo of snow. II: Snow containing atmospheric aerosols, *J. Atmos. Sci.*, *37*, 2734–2745.
- Westerling, A. L., et al. (2006), Warming and earlier spring increase western U.S. forest wildfire activity, *Science*, *313*, 940–943.
- Wooster, M. J., et al. (2003), Fire radiative energy for quantitative study of biomass burning: Derivation from the BIRD experimental satellite and comparison to MODIS fire products, *Remote Sens. Environ.*, *86*, 83–107.
- Wooster, M. J., G. Roberts, G. L. W. Perry, and Y. J. Kaufman (2005), Retrieval of biomass combustion rates and totals from fire radiative power observations: FRP derivation and calibration relationships between biomass consumption and fire radiative energy release, *J. Geophys. Res.*, *110*, D24311, doi:10.1029/2005JD006318.
- Wotawa, G., et al. (2001), Inter-annual variability of summertime CO concentrations in the Northern Hemisphere explained by boreal forest fires in North America and Russia, *Geophys. Res. Lett.*, *28*, 4575–4578.
- Yevich, R., and J. A. Logan (2003), An assessment of biofuel use and burning of agricultural waste in the developing world, *Global Biogeochem. Cycles*, *17*(4), 1095, doi:10.1029/2002GB001952.

- Yurganov, L. N., et al. (2005), Increased Northern Hemispheric carbon monoxide burden in the troposphere in 2002 and 2003 detected from the ground and from space, *Atmos. Chem. Phys.*, 5, 563–573.
- Zender, C. S., H. Bian, and D. Newman (2003), Mineral Dust Entrainment and Deposition (DEAD) model: Description and 1990s dust climatology, *J. Geophys. Res.*, 108(D14), 4416, doi:10.1029/2002JD002775.
- Zhang, L., et al. (2001), A size-segregated particle dry deposition scheme for an atmospheric aerosol module, *Atmos. Environ.*, 35, 549–560.
-
- J.-L. Attié, Laboratoire d’Aérodologie, F-31400 Toulouse, France.
- I. Bey and S. Generoso, Laboratoire de Modélisation de la Chimie Atmosphérique, Ecole Polytechnique Fédérale de Lausanne, CH-1015 Lausanne, Switzerland. (sylvia.generoso@epfl.ch)
- F.-M. Bréon, Laboratoire des Sciences du Climat et de l’Environnement, Institut Pierre Simon Laplace, F-91191 Gif-sur-Yvette, France.